A High-Order Discontinuous Galerkin Method for Optimal Control of an OWC Spar Buoy

Ricardo Filipe Gomes Duarte
ricardo.g.duarte@tecnico.ulisboa.pt

Instituto Superior Técnico, Lisboa, Portugal

January 2021

Abstract

Pseudospectral (PS) methods appeared in the 1990s and became an almost standard tool for the numerical solution of optimal control problems (OCPs). One of the fundamental characteristics of the PS methods is the ability to achieve high-order accuracy for smooth OCPs. This accuracy results from approximating the state and control trajectories by single polynomials across the entire domain. However, the high-order accuracy is usually lost for bang-bang OCPs because of the non-smooth nature of the control. The current thesis aims to study an alternative approach to PS methods: a high-order Discontinuous Galerkin Finite Element Method (DG-FEM) for the numerical solution of OCP based on Pontryagin's Maximum Principle. In contrast with the PS methods, the DG-FEM use a piecewise polynomial solution of the state and control trajectories where mesh and polynomial refinement are straightforward to implement. The application of mesh refinement allows obtaining high-order solutions even for bang-bang OCPs. To show the capabilities of the method, two test cases were considered: a continuous and a bang-bang time-solutions. A detailed study of the convergence properties of the method was performed for both cases. For that, a floating-point arithmetic library with arbitrary precision was used. The results demonstrated the expect problems of using double-precision arithmetic for polynomial approximations of degree above six. Finally, the method was successfully applied for optimal control of an OWC spar buoy wave energy converter. The results showed a 20% in the turbine output power in comparison with the standard non-optimal control.
Keywords: nonlinear optimal control, discontinuous Galerkin, shooting method, oscillating water column, Pontryagin's maximum principle

1. Introduction

The Oscillating water column principle is one of many viable ways to extract energy from ocean waves [15, 16]. This principle uses the waves' oscillation to move a water column (inside a device, either floating or fixed), which changes the air pressure between a turbine and the environment. The pressure gradient forces air through the turbine and induces its rotor movement. The rotor of the turbine is attached to an electrical energy generator, which supplies power to the grid.

Nowadays, the most common design of OWC devices uses a self rectifying turbine, i.e. a turbine that keeps its sense of rotation independently of the sense of the air flow [12], thus eliminating the need for valves to control the flow direction. The most common turbine for this purpose is the Wells turbine (with guiding vanes) [11, 4] attached to a doubly fed induction generator (DFIG). The wells turbine is used due to its simplicity and capability to deal with bi-directional flows [12]. Some designs replace the Wells turbine (reaction turbine) with an impulse turbine, which has been shown to increase the operating range with higher efficiency [12, 7]. A reaction turbine is kept rotating due to the deflection of air hitting the blades, while an impulse turbine relies on the impulse given by the fluid passing through the blades.

Recently, the Wave Energy Group of Instituto Superior Técnico (IST) developed a new self-rectifying bi-radial turbine with which proved to have a better performance than a Wells turbine, for this application [7, 12]. This turbine can be equipped with a simple high-speed stop valve that allows an open/closed operation as well as the partial closure of the valve. This thesis will only focus on the open/closed usage of the valve, which will be treated as a bang bang optimal control problem (OCP).

An upcoming method to solve OCP problems is the finite element method: Discontinuous Galerkin (DG-FEM). This FEM method was proposed by [20] as a method to solve nonlinear differential equations. In this thesis, the DG-FEM with a mesh re-

finement technique will be used with the same goal as [10] but with a different formulation, with a specific focus on the bang-bang control problems, as they are troublesome to pseudo-spectral methods.

The DG-FEM method to solve OCP problems, takes advantage of a discretization of the problem time domain element-wise and the weak form of the differential equations, which is very well known of most used finite element methods [19]. These characteristics ar combined a to achieve high order of accuracy and convergence characteristics [1]. Furthermore, the refinement of the time mesh is comes naturally and the discontinuities (like the solutions of bang-bang OCPs) are easily handled because the boundary between each element has a discontinuity.

Nowadays, the most established numerical solutions to optimal control problems, are the pseudo-spectral methods (PS), which were first introduced in the 1990s [3] and have gathered popularity, to the point of being the standard continuous-time OCP solving method, in research and industry [21]. These methods present high order of accuracy for smooth OCP [21].

The PS methods use polynomials to approximate the entire time domain of the OCP, where each polynomial used is pondered by a variable coefficient. These coefficients are computed according to the problem; using the minimization of a norm calculated in a chosen quadrature (preferably, Gauss-Lobatto or Chebyshev–Gauss–Lobatto [21]). The refinement of solutions is made by increasing the number of polynomials and the number of points in the quadrature. Since the the variables are approximated by polynomials (which are continuous and smooth), these methods are bound to have accuracy problems for discontinuous our non smooth OCPs.

1.1. Document structure

This paper is divided into 5 sections, including the introduction 1, where a small review on the oscillating water column and its control principle is present.

Section 2 presents the Spar Buoy theoretical system with a physical and numerical description of the energy transmission effects.

The third section shows the numerical methods implemented for optimal control problems with fixed terminal time and in continuous time (finite elements). First, it starts with a review of optimal control theory, then follows a review of the finite element method, specifically the Discontinuous Galerkin method (DG), and finally the integration of optimal control and finite elements. It provides the base for the next simulations where this theory is validated.

The fourth section presents the of the developed formulation is now done by solving the problem proposed by Gong et al. [18] (simple continuous PMP problem), which tests the ability to solve continuous control problems. 4.1. The problem proposed by Luenberger, D. [14] (simple bang-bang problem) is then solved, which tests the ability to solve bang-bang control problems, with mesh refinement, in this case, with one switching time instant. Then, the OWC Spar buy system is tested with 1 wave and 3 waves of different frequency.

Finally, in section 5, the conclusions about the developed work, obtained results and achievements ware displayed.

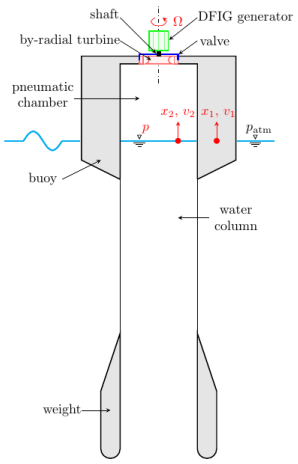

Figure 1: Cross section of the buoy scheme.

2. OWC Spar Buoy System

The OWC spar buoy system consists of a long, hollow and axisymmetric buoy with a turbine and a generator attached to its head, approximately as it is shown in figure 1 [6].

The formulation of the spar buoy dynamics present in this section mainly follows the time domain approach already developed by [22] and [9].

2.1. Hydrodynamics

The OWC spar buoy is a two-body system composed of a floater and tail tube filled with water. The floater and the OWC free-surface are denoted as body 1 and 2, respectively, as depicted in Fig. 1. For computing the hydrodynamic coefficients in the frequency domain, body 2 is modeled as an imaginary neutrally buoyant rigid piston.

The discussed model will only consider the heave motion of the buoy (up and down motion). Furthermore, it is assumed that the surface of the inside water column is plane and horizontal. The vertical position of body i is named x_i, with the x-axes pointing upward. At the equilibrium position, $x_i = 0$. With the previous assumptions, the first two equations of the buoy's dynamics, describing

the heave motion, are:

$$(m_1+A_{11}^{\infty})\ddot{x}_1 + A_{12}^{\infty}\ddot{x}_2 = -\rho_{\mathrm{w}} g S_1 x_1 + S_2 p_{\mathrm{atm}} p^* + F_{\mathrm{d}_1} - R_{11}(\dot{x}_1) - R_{12}(\dot{x}_2), \quad (1)$$

$$A_{21}^{\infty}\ddot{x}_1 + (m_2 + A_{22}^{\infty})\ddot{x}_2 = -\rho_{\mathrm{w}} g S_2 x_2 - S_2 p_{\mathrm{atm}} p^* + F_{\mathrm{d}_2} - R_{21}(\dot{x}_1) - R_{22}(\dot{x}_2), \quad (2)$$

where the mass of body i is denoted as m_i. The limiting value at infinite frequency of the added mass of body i as affected by the motion of body j is defined by A_{ij}^{∞}. The buoy and the inside OWC are under the effect of excitation F_{d_i}, radiation R_{ij}, and the hydrostatic restoring forces $\rho_w g \mathrm{S}_i x_i$, where ρ_w is the water density, g the gravity acceleration and S_i the area of the section parallel to the water surface for each body. The force resulting from the air chamber pressure is represented by the term $S_i p_{\mathrm{atm}} p^*$, p_{atm} is the atmospheric pressure, and p^* is the dimensionless relative pressure inside the air chamber defined by

$$p^* = \frac{p - p_{\mathrm{atm}}}{p_{\mathrm{atm}}}. \quad (3)$$

Here p is the absolute pressure inside the air chamber.

The radiation forces are defined by the terms $\mathrm{A}_{ij}^{\infty}\ddot{x}_j + R_{ij}$. usualy, R_{ij} are terms defined by a convolution integral. For simplification, in this thesis, R_{ij} was be calculated as viscous dampers: $R_{12} = R_{21} = 0$ and $R_{11} = c_1\dot{x}_1$, $R_{22} = c_2\dot{x}_2$.

The wave excitation forces are represented by F_{d_i}. With the assumption of linear water wave theory, it can be computed as:

$$F_{\mathrm{d}_i} = \sum_{m=1}^{N} \Gamma_i(\omega_m) A(\omega_m) \cos(\omega_m t + \phi_{i_m} + \phi_r), \quad (4)$$

i.e. the sum of several regular waves with different angular frequency. Γ_i represents the excitation force coefficient for body i, A the frequency dependent wave amplitude, ϕ_{m_i} is the frequency response of body i and ϕ_r is just a random phase [9]. $A(\omega_m)$ may be calculated with:

$$A = \sqrt{\Delta\omega_m S_{\omega_m} \omega_m}. \quad (5)$$

where S_{ω_m} is the power spectral density of the wave climate and $\Delta\omega_m$ is a frequency interval resultant from the discretization of the frequency spectrum. For a given $\Delta\omega_m$ the correspondent ω_m should be placed in the middle of the interval:

$$\omega_m = \omega_{m-1} + \frac{1}{2}(\Delta\omega_{m-1} + \Delta\omega_m). \quad (6)$$

The power spectral density S_{ω_m} may be given by Pierson-Moscowitz formula:

$$S_{\omega_m} = 262.9 \frac{H_s^2}{\omega_m^5 T_e^4} e^{-\frac{1054}{(\omega_m T_e)^4}}, \quad (7)$$

where T_e represents the wave energy period and H_s the significant wave height (which are referent to the wave climate).

To transform the system in a state space representation, let $v_1 = \dot{x}_1$ and $v_2 = \dot{x}_2$. Introducing the total mass matrix (8), the closed form of equations (1) and (2) is derived as:

$$M = \begin{bmatrix} \mathrm{m}_1 + \mathrm{A}_{11}^{\infty} & \mathrm{A}_{12}^{\infty} \\ \mathrm{A}_{21}^{\infty} & \mathrm{m}_2 + A_{22}^{\infty} \end{bmatrix} \quad (8)$$

$$\dot{v}_1 = \det(M)^{-1}\Big((m_2 + A_{22}^{\infty})\mathcal{F}_1 - A_{12}^{\infty}\mathcal{F}_2\Big), \quad (9)$$

$$\dot{v}_2 = \det(M)^{-1}\big((m_1 + A_{11}^{\infty})\mathcal{F}_2 - A_{21}^{\infty}\mathcal{F}_1\big), \quad (10)$$

$$(11)$$

$$\mathcal{F}_1 = -\rho_{\mathrm{w}} g \mathrm{S}_1 x_1 + S_2 p_{\mathrm{atm}} p^* + F_{\mathrm{d}_1} + R_{11}(v_1) + R_{12}(v_2),$$

$$\mathcal{F}_2 = -\rho_{\mathrm{w}} g \mathrm{S}_2 x_2 - S_2 p_{\mathrm{atm}} p^* + F_{\mathrm{d}_2} + R_{21}(v_1) + R_{22}(v_2).$$

2.2. Pneumatic Chamber

The pneumatic chamber is located between the water column and the turbine. For the developed model, the water column will act as a rigid "piston", whose dynamics are already described in (9) and (10) (x_1, x_2, v_1, v_2). The turbine will then acquire some of the pneumatic energy and allow the movement of mass from the system $\dot{m}_{\mathrm{t}}$ (which is defined in subsection 2.3). Below, there is a short demonstration for the dynamics equation of the pressure accounting with compressibility effects and starting on the classic continuity equation:

$$\dot{\rho}V + \rho\dot{V} = -\dot{m}_{\mathrm{t}} \quad (12)$$

The volume of the air chamber V and its variation can be defined as

$$V = (h_0 + x_1 - x_2)S_2, \quad (13)$$

where, h_0 is the height of the chamber at the equilibrium position. The compression/decompression of air is assumed to be an isentropic process and the air is modeled as a perfect gas:

$$\rho = \rho_{\mathrm{atm}} \left(\frac{p}{p_{\mathrm{atm}}}\right)^{1/\gamma} = \rho_{\mathrm{atm}}(p^* + 1)^{1/\gamma} \quad (14)$$

$$\dot{\rho} = \rho_{\mathrm{atm}} \frac{1}{\gamma}(p^* + 1)^{1/\gamma - 1}\dot{p}^* \quad (15)$$

, where γ is the specific heat ratio for air (1.4) and ρ_{atm} is the air density at atmospheric pressure.

From the algebraic manipulation of equation (12) and acknowledging the definitions in (13) and (14), results expression:

$$\dot{p}^* = -\frac{\gamma}{\rho S_2}\frac{\dot{m}_{\mathrm{t}}(p^* + 1)}{h_0 + x_1 - x_2} - \gamma\frac{(p^* + 1)(\dot{x}_1 - \dot{x}_2)}{h_0 + x_1 - x_2}. \quad (16)$$

With these expressions, the system's first nonlinearity is, finally, introduced.

2.3. Power take-off system dynamics

The final power transmission to the generator is assured by a shaft coupling turbine and generator. The dynamics equation for the rotation of the shaft is:

$$I\dot{\Omega} = T_\mathrm{t} - T_\mathrm{gen} \tag{17}$$

in which, T_t is the Torque supplied by the turbine, T_gen is the torque absorbed by the generator, I is the moment of inertia along the axis of rotation and Ω is the rotational speed of the shaft. T_t and T_gen are usually a function of the flow characteristics, and type of devices and their size. It is typical, when dealing with turbo-machines such as the bi-radial turbine, to normalize the variables, by the characteristics of the flow and the machine (like the rotor diameter d). The expressions for the dimensionless pressure head Ψ, flow Φ and power Π are:

$$\Psi = \frac{p^* p_\mathrm{atm}}{\rho_\mathrm{t} \mathrm{d}^2 \Omega^2} \qquad \Phi = \frac{\dot{m}_\mathrm{t}}{\rho_\mathrm{t} \mathrm{d}^3 \Omega} \qquad \Pi = \frac{P_\mathrm{t}}{\rho_\mathrm{t} \mathrm{d}^5 \Omega^3} \tag{18}$$

$$p^* = \frac{\Psi \rho_\mathrm{t} \mathrm{d}^2 \Omega^2}{p_\mathrm{atm}} \qquad \dot{m}_\mathrm{t} = \rho_\mathrm{t} d^3 \Omega \qquad P_\mathrm{t} = \Pi \rho_\mathrm{t} \mathrm{d}^5 \Omega^3 \tag{19}$$

For the dimensionalization just apply the inverse transformation (19), being p^* the non dimensional pressure, $\dot{m}_\mathrm{t}$ the mass air flow and P_t the turbine power. To obtain T_t for expression (17) remember that $T_\mathrm{t} = \frac{P_\mathrm{t}}{\Omega}$. In these expressions, the term ρ_t is also present; this air density is different from ρ in the air chamber (16, since it is correspondent to the density of the inlet/outlet of air through the turbine:

$$\rho_\mathrm{t} = \begin{cases} (p^* + 1)^{\frac{1}{\gamma}} \rho_\mathrm{atm}, p^* > 0 \\ \rho_\mathrm{atm}, \text{ otherwise} \end{cases} \tag{20}$$

To calculate T_t and $\dot{m}_\mathrm{t}$ the data from [5] can be used. The expressions used to model the turbine for the bang-bang problem were:

$$\hat{\Phi}(\Psi, u) = \frac{0.12695\Psi^4 - 0.71\Psi^3 + 5.068\Psi^2 + 4.289\Psi}{\Psi^3 - 2.561\Psi^2 + 37.46\Psi + 6.278} \tag{21}$$

$$\hat{\Pi}(\Phi) = -272\Phi^{10} + 252\Phi^8 - 84.26\Phi^6 + 12.9\Phi^4 + 2.605\Phi^2 - 0.00657 \tag{22}$$

Without the effect of partial valve closure the control problem may be transformed into a specific type of on-off control: bang-bang control problem. For these types of problems, the state function and the objective function need to be linear with the control [13].

The control for the buoy is the valve u, with $u = 1$ corresponding to the open valve and $u = 0$ to the closed valve. The adapted problem for the application of the bang-bang principle requires

$$T_\mathrm{t} = u\Pi\Omega^2 \mathrm{d}^5 \rho_\mathrm{t} \tag{23}$$

$$\dot{m}_\mathrm{t} = u\Phi\Omega \mathrm{d}^3 \rho_\mathrm{t} \tag{24}$$

and for the maximization of the turbine power

$$P_\mathrm{t} = u\Pi\Omega^3 \mathrm{d}^5 \rho_\mathrm{t}. \tag{25}$$

Regarding the generator electromagnetic torque, equation (19) shows that the turbine output power should be proportional to Ω^3 if the time-averaged turbine aerodynamic efficiency is to be maximized. In practice, if the coupling between the turbine aerodynamics and the spar-buoy OWC hydrodynamics is taken into account, we can use a relation of the type [8]

$$P_\mathrm{gen}^\mathrm{opt} = a\Omega^b, \tag{26}$$

where b is about 3 (in fact 3.33 was used) and the constant a used was 0.025. To obtain the torque for the optimal power, just aknowledge that

$$T_\mathrm{gen} = P_\mathrm{gen}/\Omega = a\Omega^{b-1} \tag{27}$$

3. Optimal Control Solution Using a Discontinuous Galerkin Finite ElementMethod

3.1. Optimal Control Theory

The original Pontryagin's Maximum Principle (PMP) focuses on finding an optimal path for a set of variables for the maximization of a specified performance index J given by a final state cost $\mathbf{c}_f$ and a Lagrangian function $\mathcal{L}$ pondered over time. This originates the problem described by the following expressions [13][22]:

Maximize:

$$J = c_f\big(\mathbf{x}(t_f)\big) + \int_{t_0}^{t_f} \mathcal{L}(t, \mathbf{x}, \mathbf{u})\, \mathrm{d}t, \tag{28}$$

subject to:

$$\dot{\mathbf{x}} = \mathbf{f}(t, \mathbf{x}, \mathbf{u}) \tag{29}$$

and the boundary condition:

$$\mathbf{x}(t_0) = \mathbf{x}_0, \tag{30}$$

where $\mathbf{x}$ is the array of state variables, $\mathbf{u}$ are the control variables and t is the time. c_f is the cost associated with final states, t_0 and t_f are the initial and final time of the problem respectively. The Hamiltonian function can be defined as

$$\mathcal{H} = \mathcal{L}(t, \mathbf{x}, \mathbf{u}) + \boldsymbol{\lambda}^T \mathbf{f}(t, \mathbf{x}, \mathbf{u}) \tag{31}$$

Instead of showing the extensive demonstration of the the PMP formulation, the main results are:

$$\dot{\mathbf{x}} = \nabla_{\boldsymbol{\lambda}} \mathcal{H}(t, \mathbf{x}, \mathbf{u}, \boldsymbol{\lambda}), \tag{32}$$

$$\dot{\boldsymbol{\lambda}} = -\nabla_{\mathbf{x}} \mathcal{H}(t, \mathbf{x}, \mathbf{u}, \boldsymbol{\lambda}), \tag{33}$$

$$\mathbf{u} : \mathcal{H} = \max(\mathcal{H}), \tag{34}$$

$$\boldsymbol{\lambda}(t_f) = \nabla_{\mathbf{x}(t_f)} c_f\big(\mathbf{x}(t_f)\big). \tag{35}$$

All these conditions apply if $\mathbf{u}$ is optimal. [22] shows a comprehensible demonstration to these statements. This suggest the PMP can be solved in 3 stages stages: solving the state variables, through expression (32); solving the co-state variables, with the solution of (33) (Lagrange multipliers) and solving the optimal control equation (34) where (35) is the boundary condition.

With a boundary condition placed at t_f the most natural way to solve equation (33) is to integrate it backwards in time (from t_f to t_0). The first method proposed in this thesis for the PMP problem is to solve the control and the state variables forward in time and then solving the co-state variables backward (iteratively).

An alternative to the forward and backward integration can be found in book [13]. Where the problem is treated as a two-point boundary condition differential equation problem. This formulation is also developed in this paper [17].

3.2. Discontinuous Galerkin Finite Element Method

The problem depicted in the previous sub-section 3.1 requires the solution for two vectorial differential equations which describe a system in state-space form: (32) and (33). These equations do not always have an analytical solution or the solution may be less accurate or convenient than the numerical. So for that purpose, on the course of this work, the Discontinuous Galerkin (DG) finite element method will be used [19, 1], whose formulation can be followed in (36) through (46), for a generic state-space system (36).

3.2.1 DG Formulation

Assume there is a system formulated by equation (36). Recall that: $\mathbf{x}$ is the array of state variables; $\mathbf{u}$ is the array of control variables; t is the time and $\mathbf{f}$ is the state function (vectorial function with the same length as $\mathbf{x}$), which in expression (36) is nonlinear and time-dependent.

$$\dot{\mathbf{x}} = \mathbf{f}(\mathbf{x}, \mathbf{u}, t), \text{where } \mathbf{u}(t) \text{ is known.} \tag{36}$$

Multiplying (36) by a continuous smooth function v and integrating along the domain (t_0 to t_f):

$$\int_{t_0}^{t_f} \dot{\mathbf{x}}\mathbf{v}\,\mathrm{d}t = \int_{t_0}^{t_f} \mathbf{f}\mathbf{v}.\,\mathrm{d}t \tag{37}$$

Defining now an approximation for $\mathbf{x}$ as

$$\hat{\mathbf{x}}(t) = \sum_{e=1}^{n_{\text{elem}}} \tilde{\mathbf{x}}^e(t), \tag{38}$$

$$\tilde{\mathbf{x}}^e(t) = \begin{cases} \mathbf{C}^e\mathbf{p}(\tau^e) & \text{, if } t_{\text{st}}^e < t < t_{\text{st}}^e + \Delta t^e \\ \mathbf{0} & \text{, otherwise} \end{cases}, \tag{39}$$

with:

$$\mathbf{C}^e = c_{i,j}^e, \qquad 1 \le i \le n_{\text{x}}, \tag{40}$$

$$\mathbf{p}(\tau^e) = p_j(\tau^e), \qquad 0 \le j \le n_{\text{p}}, \tag{41}$$

$$\tau^e = \frac{2t - t_{\text{st}}^e - t_{\text{f}}^e}{\Delta t^e}, \tag{42}$$

$$\Delta t^e = t_{\text{f}}^e - t_{\text{st}}^e, \tag{43}$$

where $\mathbf{p} = p_i$ (polynomials of degree i, $0 \le i \le n_{\text{p}}$) and n_{p} the number of polynomials (which affects the quality of the approximation), t_{st}^e is the starting time of element e, t_{f}^e the final time and Δt^e the time interval covered by element e, also, n_{x} represents the number of state variables. τ^e, the local time, is defined in expression (42). Matrix $\mathbf{C}^e$ contains constants where each line corresponds to the approximation of one $\mathbf{x}$ and each column multiplies with a polynomial of a certain degree, as shows equation (39).

Function $\mathbf{v}$ is approximated by a set containing the same polynomials as the ones used in the approximation ($\tilde{\mathbf{v}} = p_i$). Substituting, as well, $\mathbf{x}$ in (37) by (39), divides the integral by elements. The calculations for each element are:

$$\frac{\Delta t^e}{2}\int_{-1}^{1} \frac{2}{\Delta t^e}\tilde{\mathbf{x}}^e\tilde{\mathbf{v}}^{\mathrm{T}}\,\mathrm{d}\tau^e = \frac{\Delta t^e}{2}\int_{-1}^{1} \tilde{\mathbf{f}}^e\tilde{\mathbf{v}}^{\mathrm{T}}\,\mathrm{d}\tau^e. \tag{44}$$

The left hand side of the equation integrated by parts originates the boundary condition. Rearranging the terms we get the final expressions (per element) (45), for forward integration and (46), for backwards integration.

$$-\tilde{\mathbf{x}}^e(1)\big(\tilde{\mathbf{v}}(1)\big)^{\mathrm{T}} + \int_{-1}^{1} \tilde{\mathbf{x}}^e\dot{\tilde{\mathbf{v}}}^{\mathrm{T}}\,\mathrm{d}\tau^e = - \int_{-1}^{1} \mathbf{f}(\tilde{\mathbf{x}}^e, \mathbf{u}, \tau^e)\tilde{\mathbf{v}}^{\mathrm{T}}\,\mathrm{d}\tau^e - \hat{\mathbf{x}}(t_f^{e-1})\big(\tilde{\mathbf{v}}(-1)\big)^{\mathrm{T}}, \tag{45}$$

$$\tilde{\mathbf{x}}^e(-1)\big(\tilde{\mathbf{v}}(-1)\big)^{\mathrm{T}} + \int_{-1}^{1} \tilde{\mathbf{x}}^e\dot{\tilde{\mathbf{v}}}^{\mathrm{T}}\,\mathrm{d}\tau^e = - \int_{-1}^{1} \mathbf{f}(\tilde{\mathbf{x}}^e, \mathbf{u}, \tau^e)\tilde{\mathbf{v}}^{\mathrm{T}}\,\mathrm{d}\tau^e + \hat{\mathbf{x}}(t_0^{e+1})\big(\tilde{\mathbf{v}}(1)\big)^{\mathrm{T}}. \tag{46}$$

In equation (45), $\hat{\mathbf{x}}(t_f^{e-1})$ is the approximation of $\mathbf{x}$ evaluated at the end of the previous element ($\tilde{\mathbf{x}}^{e-1}(1)$). On the other hand, in (46), $\hat{\mathbf{x}}(t_0^{e+1})$ represents the approximation of $\mathbf{x}$ calculated at the beginning of the next element ($\tilde{\mathbf{x}}^{e+1}(-1)$).

3.2.2 Linear System Simulation with DG

Expressions (47) and (48) represent the calculations that are required for the simulation of a linear system of the type $\dot{\mathbf{x}} = \mathbf{A}(t)\mathbf{x} + \mathbf{B}(t)$, derived from (45)

and (46) respectively.

$$\Big(\mathbf{P}(1)+\mathbf{D}+\frac{\Delta t^e}{2}\mathbf{I}_A\Big)\mathbf{a} = -\frac{\Delta t^e}{2}\mathbf{I}_B+\mathbf{BC}(-1)\hat{\mathbf{x}}(t_f^{e-1}), \quad (47)$$

$$\Big(\mathbf{P}(-1)-\mathbf{D}-\frac{\Delta t^e}{2}\mathbf{I}_A\Big)\mathbf{a} = \frac{\Delta t^e}{2}\mathbf{I}_B+\mathbf{BC}(1)\hat{\mathbf{x}}(t_0^{e+1}), \quad (48)$$

The following definitions are being used:

$$\begin{aligned}
&\mathbf{\Phi}(\tau)=\mathbf{p}(\tau)\big(\mathbf{p}(\tau)\big)^{\mathrm{T}};\ \mathbf{M}=\int_{-1}^{1}\dot{\mathbf{p}}\mathbf{p}^{\mathrm{T}}d\tau,\\
&\mathbf{P}(\tau)=\mathrm{diag}(\mathbf{\Phi}(\tau),\cdots,\mathbf{\Phi}(\tau)),\ n_{\mathrm{x}}\text{ blocks},\\
&\mathbf{D}=\mathrm{diag}(\mathbf{M},\cdots,\mathbf{M}),\ n_{\mathrm{x}}\text{ blocks},\\
&\mathbf{I}_A=\int_{-1}^{1}\mathbf{\Phi}\mathbf{A}_{i,j}\,\mathrm{d}\tau\ ;\\
&\mathbf{I}_B=\int_{-1}^{1}\mathbf{p}B_i\,\mathrm{d}\tau\ ;\ 1\le i\le n_{\mathrm{x}},\ 1\le j\le n_{\mathrm{x}},\\
&\mathbf{BC}(\tau)=\mathrm{diag}(\mathbf{p}(\tau),\cdots,\mathbf{p}(\tau)),\ n_{\mathrm{x}}\text{ blocks};\\
&\mathbf{a}=\begin{bmatrix}\mathbf{c}_1^{\mathrm{T}} & \cdots & \mathbf{c}_{n_{\mathrm{x}}}^{\mathrm{T}}\end{bmatrix}^{\mathrm{T}},
\end{aligned} \quad (49)$$

in which n_{x} represents the number of state variables, $\mathrm{diag}(\phi), n_{\mathrm{x}}$ blocks is a block diagonal matrix where the block ϕ is repeated n_{x} times. $\mathbf{a}$ represents the matrix of constants $\mathbf{C}$ from expression (39), but the constants are positioned in vector form: the first entries of $\mathbf{a}$, 0 up to n_{p} are the constants of x_1, then from $n_{\mathrm{p}}+1$ up to $2n_{\mathrm{p}}+1$ are constants of x_2 and so on.

3.2.3 Nonlinear System Simulation with DG

In nonlinear systems, the simulation method is bound to be iterative. Expressions (50) and (51) show the equations to solve (for $\mathbf{a}$) for forward and backward simulation.

$$\Big(\mathbf{P}(1)+\mathbf{D}\Big)\mathbf{a}=-\frac{\Delta t^e}{2}\mathbf{I}_f+\mathbf{BC}(-1)\hat{\mathbf{x}}(t_f^{e-1}) \quad (50)$$

$$\Big(\mathbf{P}(-1)-\mathbf{D}\Big)\mathbf{a}=\frac{\Delta t^e}{2}\mathbf{I}_f+\mathbf{BC}(1)\hat{\mathbf{x}}(t_0^{e+1}) \quad (51)$$

Using the definitions in (49) and (52).

$$\mathbf{I}_f=\int_{-1}^{1}\mathbf{p}f_i\,\mathrm{d}\tau\ ;\ 1\le i\le n_x. \quad (52)$$

The method chosen to solve these nonlinear vector expressions is the fixed point method. This method suggests that for iteration k the next guess for solution is calculated using $\mathbf{a}^{k+1}=\mathbf{g}(\mathbf{a}^k)$ Furthermore, with this method is possible to assure convergence for Δt^e low enough and a close enough initial guess [2].

3.3. Solving PMP Problems with DG

As seen above PMP problems require the solution of two differential equations (32)-(33), one for the state variables $\mathbf{x}$ and one for the co-state variables $\boldsymbol{\lambda}$. Unfortunately these cannot be solved together, as $\boldsymbol{\lambda}$ requires the knowledge of the control and state variables variables ($\mathbf{u}$ and $\mathbf{x}$) at the final time T, since its boundary condition is positioned there (at $t=T$) for specified initial states and fixed time problems.

In (32), $\mathbf{f}$ may be a nonlinear expression, leading to the iterations defined in the previous section 3.2.3. Looking at expressions (33) and (31), it is possible to infer that $\boldsymbol{\lambda}$ is defined by a linear, time-dependent system (53), which is easier to solve using the expressions defined for DG linear backwards simulation, present in expression (48).

$$\dot{\boldsymbol{\lambda}}=\Big(\boldsymbol{\mathcal{J}}_{\mathbf{f}}(\mathbf{x})\Big)^{\mathrm{T}}\boldsymbol{\lambda}+\nabla_{\mathbf{x}}J, \quad (53)$$

in which $\boldsymbol{\mathcal{J}}_{\mathbf{f}}(\mathbf{x})$ stands for the Jacobian of $\mathbf{f}$ about $\mathbf{x}$, i.e. $\frac{\mathrm{d}f_i}{\mathrm{d}x_j}$.

Regarding equation (34), it represents the maximization of the Hamiltonian $\mathcal{H}$ about the control variables $\mathbf{u}$, which can be solved with an optimization algorithm. In this work, the optimization algorithm used was the conjugate gradient (of *python*'s toolbox *scipy*, "cg")) for continuous control problems, but any other would do (attending to the characteristics of the problem). For *on-off* control problems, an exhaustive search is valid because all that is required is a solution using one of 2 values.

3.4. Solving PMP Problems with DG and Shooting Method

In the previous sub-section 3.3 a method is discussed to solve the PMP problem, using the DG method, by going forwards (to calculate $\hat{\mathbf{x}}$ and $\hat{\mathbf{u}}$) and backwards (to calculate $\hat{\boldsymbol{\lambda}}$) because the boundary conditions for $\boldsymbol{\lambda}$ are positioned in the final time.

In this section an alternative method is discussed, where everything is calculated forward, making the problem, possibly, faster to solve and with a better convergence: the shooting method [17].

The shooting method is mainly used to solve differential equations with boundaries in an initial time and at a final time. A typical problem of application is described in equation (54), where, to a N-th order differential equation (described as a system of first-order differential equations), there are n_1 boundary conditions placed at $t=0$ and

$n_2 = N - n_1$ boundary conditions placed at $t = T$.

$$\begin{aligned} &\frac{\mathrm{d}\mathbf{x}}{\mathrm{d}t} = \mathbf{f}(t, \mathbf{x}), \\ &x_i(t=0) - x_i^{\mathrm{BC}(t=0)} = 0 \qquad\qquad i = 1, \cdots, n_1, \\ &x_j(t=T) - x_j^{\mathrm{BC}(t=T)} = 0 \quad j = n_1 + 1, \cdots, N. \end{aligned} \tag{54}$$

This method consists on guessing the value of the variables with boundary conditions at $t = T$ in $t = 0$ (aiming), which will be imposed as a condition at $t = 0$. Then the problem can be solved with forward integration to reach T (shooting). If the initial guess for $x_j^{\mathrm{BC}(t=0)}$ is not the exact solution at $t = 0$, then there will be a discrepancy between $x_j(T)$ and the original boundary condition $x_j^{\mathrm{BC}(t=T)}$. For the purpose of the formulation let $\mathbf{V}$ be the guess of the imposed value of x_j in $t = 0$ and $\mathbf{F}$ the discrepancies, computed as $F_j = x_j - x_j^{\mathrm{BC}(t=T)}$.

3.5. Aiming

While the first value of $\mathbf{V}$ may be arbitrary, a way is required to renew the imposed initial value to restart the cycle. The used method for this work is the Newton method as suggested by [17]. A new step is calculated as

$$\mathbf{V}^{\mathrm{new}} = \mathbf{V}^{\mathrm{old}} - \left(\mathcal{J}_{\mathbf{F}}\mathbf{V}\right)^{-1}\mathbf{F}. \tag{55}$$

Unfortunately, the Jacobian $\mathcal{J}_{\mathbf{F}}\mathbf{V}$ required for the calculations is usually not available. So, these should be calculated as numerical Jacobians:

$$(\mathcal{J}_{\mathbf{F}}\mathbf{V})_{ij} = \frac{\Delta F_i}{\Delta V_j} = \frac{F_i(\mathbf{V} + \delta V_j) - F_i(\mathbf{V})}{\delta V_j}. \tag{56}$$

Keep in mind the calculation of the Jacobian requires the integration of the problem n_2 extra times (one time for each δV_j). Then, each step for the shooting iterations, requires $n_2 + 1$ solutions for the problem accounting for the original calculation of $\mathbf{F}$.

4. Tests and Results

The calculation of the error in these plots corresponds to the L^2 norm, as defined by [1]:

$$||\mathrm{error}(\phi)||_2 = \sqrt{\frac{1}{T}\int_0^T (\phi(t) - \hat{\phi}(t))^2 \,\mathrm{d}t} \tag{57}$$

Remember that $\hat{\phi}$ is the approximation of ϕ by (38), on the other hand ϕ is the exact solution of the problem.

4.1. Test Case: Continuous Control

As mentioned before, [10] already solved this problem numerically with a slightly different formulation. They achieved an order of convergence of about $n_{\mathrm{p}} + 0.5$, even though. This problem required a relaxation factor in order to converge with the forward ad backward integration: $\tilde{\mathbf{x}}^e = \omega\tilde{\mathbf{x}}^{e^{\mathrm{new}}} + (1 - \omega)\tilde{\mathbf{x}}^{e^{\mathrm{old}}}$, where, after each calculation of the state variables with the fixed point method, the state variables before the fixed point $\tilde{\mathbf{x}}^{e^{\mathrm{old}}}$ will be added to the state variables calculated $\tilde{\mathbf{x}}^{e^{\mathrm{new}}}$, through a relaxation factor $0 < \omega \leq 1$.

The maximization of the Hamiltonian for continuous control is being achieved with the conjugate gradient from *scypy* toolbox.

4.1.1 Problem Statement

Maximize:

$$J(u) = \int_0^{\mathrm{T}} -u^2 dt - 4x_1(T) - x_2(T) \tag{58}$$

subject to

$$\begin{cases} \dot{\mathbf{x}} = \begin{pmatrix} x_2^3 & , & u \end{pmatrix} \\ \mathbf{x}(0) = \begin{pmatrix} 0 & , & 1 \end{pmatrix} \\ T = 2 \end{cases} \tag{59}$$

4.1.2 Results: Numerical Errors and Error Trend-lines

In this problem it was still possible to implement the integrals as symbolic; consequently, the numerical deviations from the analytical solution may only be caused by the DG method or the maximum precision of the operations. Figure 2 shows the variation of the numerical absolute error (square norm) with polynomial degree n and elements time interval Δt^e, with arbitrary precision (number of decimal places (dps) = 100(2(a)), 8(2(b)) or 16(2(c)). These figures were obtained using the forward and backward integration method. Figure 2(d) is obtained with the shooting method. In these figures markers are the points calculated, lines are the trend-lines of the absolute error (with slope p). Note the log-log scale.

4.2. Test Case: Bang-bang Control

As referenced before [13], bang-bang problems are on-off problems with the particularity of having a functional and a state space equation linear with u. Looking at (60) and (61) it is evident that this problem is a bang-bang control problem.

The algorithm to solve bang-bang problems was equiped with a mesh refinement method. This method consists on refining the mesh in the case that $\partial\mathcal{H}/\partial u$ changes sign between the right and left boundaries of one element. A sign change on $\partial\mathcal{H}/\partial u$ symbolizes (for continuous functions) a change in the control.

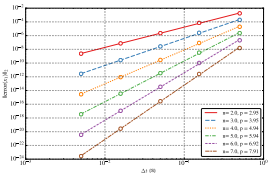

(a) Calculated with 100 decimal places

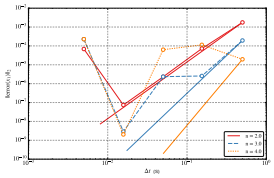

(b) Calculated with 8 decimal places

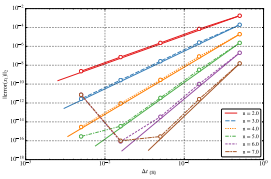

(c) Calculated with 16 decimal places

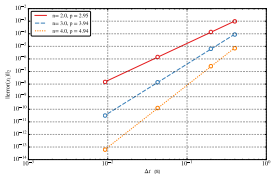

(d) Using shooting method and 100 decimal places

Figure 2: Root mean square error and trend as function of Δt and the polynomial degree n (where p is the slope of the trend line).

[10] also solved this problem with the slightly different formulation and obtained a convergence of the error of the order of about $n_{\mathrm{p}} + 0.5$. Unlike the continuous problem, this did not require the relaxation factor for the forward and backward integration algorithm, nor the shooting method.

4.2.1 Problem Statement

Maximize:

$$J(u) = \int_0^{\mathrm{T}} (1-u)x dt \tag{60}$$

subject to:

$$\begin{cases} \dot{x} = (u - 0.5)x \\ x(0) = 1 \\ T = 5 \end{cases} \tag{61}$$

4.2.2 Results: Numerical Errors and "Switching time" Error

To avoid the complications of the continuous problem in the previous section, these calculations were made with $dps = 100$. Figure 3(a) shows the error considering t_{s} to be a part of the boundary of two elements.

On the other hand, figures 4a and 4b represent the error considering t_{s} to be inside one element. In figure 4a, t_{s} is in the middle of an element. In figure 4b, t_{s} is located at a distance of 5% of element length from the element's right boundary.

Finally, figure 3(b) represents the error as a function of the initial element size and the polynomial degree of the solution found using the shooting method with refinement and figure 5 shows a sensitivity test made to the shotting method algorithm.

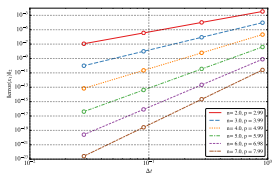

(a) Forwards and backwards method

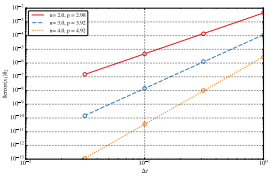

(b) shooting method

Figure 3: Root mean square error with refinement

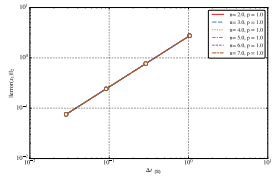

(a)

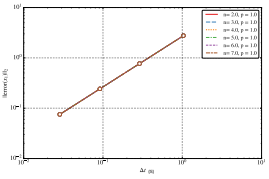

(b)

Figure 4: Error of simulation with t_{s}: (a) at 50% of element length, (b) at 5% of element length from the left boundary.

4.3. Results: OWC Spar Buoy

The First test shown, is made with the excitation force in 6. This excitation force was build to validate the system and force a symmetrical behavior of the control. The resultant control can be found in figure 7.

The second test, is done for an irregular wave environment with three waves, where the excitation force is in figure 8.

5. Conclusions

The present article applied a Discontinuous Galerkin Finite Element Method (DG-FEM) to solve nonlinear optimal control problems based on Pontryagin's Maximum Principle. The methodology was extensively tested with arbitrary precision and refinement problems. The DG-FEM can be viewed as an alternative to the established spectral methods [21]. Pontryagin's Maximum Principle DG-FEM has several advantages, namely the possibility of easily handling discontinuous control, as the control and the ability to use mesh refinement techniques to improve the accuracy. The spectral methods handle mesh refinement by adjusting the number of points and their global position of the mesh. However, the approximation of the solution spans across the computational domain. On the other hand, DG-FEM based algorithms are significantly more versatile than the spectral methods. This method allows a simple implementation of local mesh and polynomial refinement (*hp*-refinement). The mesh refinement is based on element subdivision, while polynomial refinement uses the adjustment of the degree of the

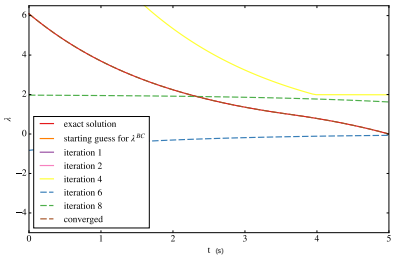

Figure 5: Sensitivity analysis of the shooting method.

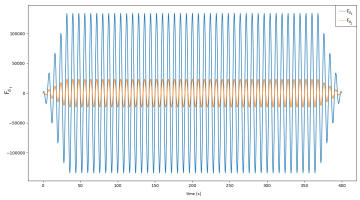

Figure 6: Altered excitation force

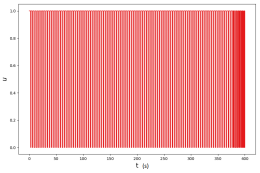

(a) Control for figure 6

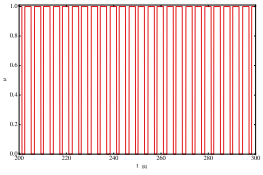

(b) Control for figure 6 zoomed

Figure 7: Control with excitation force in 6.

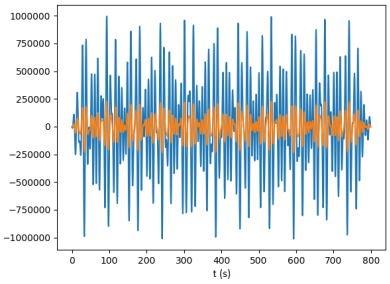

Figure 8: Excitation force with 3 wave periods.

polynomial approximation within each element according to a specified criterion. Another important difference between the spectral methods and the proposed methodology concerns the maximization of the Hamiltonian. With spectral methods, the maximization is ensured at specific control points. The DG-FEM guarantees the maximization of the Hamiltonian using an integral approach that uses an element-wise continuous solution.

In this paper, the mesh refinement in bang-bang optimal control problems was explored. An iterative approach was implemented to compute the switching instant. The results showed that it was possible to compute the switching points within the prescribed accuracy and, moreover, it was also demonstrated that the convergence was $p+1$, where p is the order of the polynomial. This is an improvement in comparison with previous results published in [10], where the order of convergence was $p+1/2$. This was due to a change in the DG-FEM formulation. The shooting method was also explored as a viable way to solve these problems. It performed well under all the test problems as well as the sensitivity analysis made to the admissible values of the arbitrary initial boundary condition. But, inconclusively, this was not possible to apply to the OWC Spar buoy system.

Another important result was the demonstration that double precision (15 significant digits) is not enough to compute accurate solutions for high-order polynomial approximations. The results obtained in this thesis used a prescribed number of significant digits, typically 100, such that the order of convergence was always $p+1$ independently of the mesh size.

The optimal control of an OWC spar buoy wave energy converter (WEC) was also implemented following the previous works made by the IST Wave Energy Group. The goal was to implement the so-called "Latching or phase control" of the WEC to maximize the power extraction. This is done by performing an optimal bang-bang control of a high-speed stop valve installed in series with the turbine rotor. The results presented for the studied OWC spar buoy showed several improvements when compared to previous published results [10]. The chattering phenomenon was largely reduced even without a regularization term used in [10] to penalize the closing of the valve. Furthermore, the optimal control achieved a 20% of increase in the generated turbine power, in comparison with the uncontrolled scenario.

References

[1] M. Baccouch. Analysis of a posteriori error estimates of the discontinuous Galerkin method for nonlinear ordinary differential equations. *Applied Numerical Mathematics*, 106:129–153, 2016.

[2] R. L. Burden and J. D. Faires. *Numerical Analysis*. Brooks/Cole Cengage Learning, 9th edition, 2011.

[3] G. Elnagar, M. A. Kazemi, and M. Razzaghi. The pseudospectral legendre method for discretizing optimal control problems.

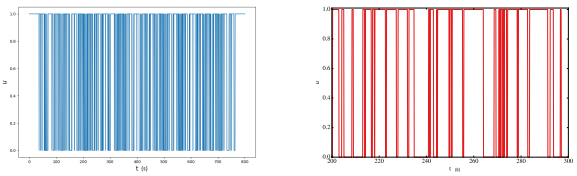

(a) Control for figure 8

(b) Control for figure 8 zoomed

Figure 9: Control with excitation force in 8.

IEEE Transactions on Automatic Control, 40(10):1793–1796, 1995.

[4] A. F. O. Falcão, J. C. C. Henriques, and L. M. C. Gato. Self-rectifying air turbines for wave energy conversion : A comparative analysis. *Renewable and Sustainable Energy Reviews*, 91(January):1231–1241, 2018.

[5] A. F. O. Falcão, L. M. C. Gato, and E. P. A. S. Nunes. A novel radial self-rectifying air turbine for use in wave energy converters. part 2. results from model testing. *Renewable Energy*, 53:159 – 164, 2013.

[6] A. F. O. Falcão, J. C. C. Henriques, and J. J. Cândido. Dynamics and optimization of the owc spar buoy wave energy converter. *Renewable Energy*, 48:369 – 381, 2012.

[7] A. F. O. Falcão, J. C. C. Henriques, and L. M. C. Gato". Oscillating-water-column wave energy converters and air turbines: A review. *Renewable Energy*, 85:1391–1424, 01 2016.

[8] A. F. de O. Falcão. Control of an oscillating-water-column wave power plant for maximum energy production. *Applied Ocean Research*, 24(2):73 – 82, 2002.

[9] J. C. C. Henriques, A. F. de O. Falcão, R. P. F. Gomes, and L. M. C. Gato. Latching control of an OWC spar-buoy wave energy converter in regular waves. In *International Conference on Offshore Mechanics and Arctic Engineering*, volume 44915, pages 641–650. American Society of Mechanical Engineers, 2012.

[10] J. C. C. Henriques, J. M. Lemos, L. Eça, L. M. C. Gato, and A. F. O. Falcão. A high-order Discontinuous Galerkin Method with mesh refinement for optimal control. *Automatica*, 85:70–82, 2017.

[11] J. C. C. Henriques, J. C. C. Portillo, W. Sheng, L. M. C. Gato, and A. F. O. Falcão. Dynamics and control of air turbines for oscillating water columns : Case study. *Renewable and Sustainable Energy Reviews*, 112:571–589, 2019.

[12] T. Karthikeyan, A. Samad, and R. Badhurshah. Review of air turbines for wave energy conversion. In *2013 International Conference on Renewable Energy and Sustainable Energy (ICRESE)*, pages 183–191, 2013.

[13] F. L. Lewis, D. Vrabie, and V. L. Syrmos. *Optimal Control*. John Wiley & Sons, inc., 3rd edition, 2012.

[14] D. G. Luenberger. *Introduction to dynamic systems: theory, models, and applications*. J. Wiley & Sons, New York, Chichester, Brisbane, 1979.

[15] A. F. de O Falcão. Wave energy utilization : A review of the technologies. *Renewable and Sustainable Energy Reviews*, 14:899–918, 2009.

[16] M. Penalba and J. V. Ringwood. A Review of Wave-to-Wire Models for Wave Energy Converters. *Energies*, 9, 2016.

[17] W. H. Press, J. C. A. Wevers, B. P. Flannery, S. A. Teukolsky, W. T. Vetterling, B. Flannery, and W. T. Vetterling. *Numerical Recipes in C: The Art of Scientific Computing*. Number v. 1 in Numerical Recipes in C book set. Cambridge University Press, 1992.

[18] Qi Gong, Wei Kang, and I. M. Ross. A pseudospectral method for the optimal control of constrained feedback linearizable systems. *IEEE Transactions on Automatic Control*, 51(7):1115–1129, July 2006.

[19] J. N. Reddy. *Introduction to the finite element Method*. McGraw-Hill, 3rd edition, 2006.

[20] W. H. Reed and T. R. Hill. Triangular mesh methods for the neutron transport equation. Technical report, University of California, Los Alamos Scientific Laboratory, 1973.

[21] I. M. Ross and M. Karpenko. A review of pseudospectral optimal control: From theory to flight. *Annual Reviews in Control*, 36(2):182 – 197, 2012.

[22] J. N. H. Valério. Dimensionamento e controlo do sistema de conversão de energia de um dispositivo de flutuante de aproveitamento de energia das ondas baseado no princípio da coluna de água oscilante. Master's thesis, Instituto superior técnico, 2017.